

Improving Stand-Alone Hybrid Generation System Using Sliding Mode Control Approach

Ridha Benadli^{1*}, Brahim Khiari¹, Marwen Bjaoui¹, Anis Sellami²

¹LANSER Laboratory/CRTEn B.P.95 Hammam-Lif 2050, Tunis-Tunisia

²Research unit: LISIER, National Higher Engineering School of Tunis, Tunis-Tunisia

*corresponding author: ridhabenadly@gmail.com

Abstract – This paper presents a robust sliding mode control (SMC) to improve the power quality of a stand-alone hybrid power system. The considered hybrid system includes photovoltaic (PV), wind turbine (WT) based on permanent magnet synchronous generator (PMSG) and battery energy storage systems (BESS). The optimization of the photovoltaic system is powered by a set of Adaptive Perturbation and Observation Algorithm Method (APOAM) to search optimum working of this source. A SMC is utilized to manage the PV voltage to achieve the Maximum Power Point (MPP) by altering the obligation duty cycle. For the wind generation system, a maximum power extraction based on a SMC is proposed for the permanent magnet synchronous generator (PMSG). This study develops non-linear controllers with an SMC method for a PV/Wind/battery system including a boost converter, bidirectional buck-boost converter and voltage source inverter (VSI). Performance verification in MATLAB/Simulink have obviously exhibited the robustness and the performance of the control strategies developed for the power converters framework compared with the conventional PI controller. It is observed from the simulation results that the average THD value is very small compared to the PI controller, around 3.1% compared to 3.91%. Hence, the power quality and the stability of the whole hybrid system are widely improved using SMC compared to other classical PI techniques.

Keywords: sliding mode control, hybrid renewable energy system, maximum power point tracking, power quality, grid connected systems

Article History

Received 17 July 2021

Received in revised form 22 August 2021

Accepted 8 September 2021

I. Introduction

The combination of renewable energy sources allows for better energy availability and optimizes maximum power generation systems, and one or more devices storage ensure the availability of energy. Among the renewable energy sources, photovoltaic and wind have interesting possibilities for exploitation at competitive costs and combining these two sources will ensure continuity of production of electrical energy and limit the climate factors dependency since they have the advantage of complementing each other.

In this context, the stand-alone hybrid renewable energy systems (HRES) was presented previously by few researchers [1]-[6], where the authors have been studying the modeling and control of this system. Several convincing results can be found in these works, however, the authors have not applied intelligent techniques for power converters. The HRES studied has a dynamic behaviour that depends on several factors, which are: the

system constraints and the appearance of defects (i.e. sudden load change, unbalanced load, and nonlinear load). In these RES applications, the control technique commonly used for power converters is the PI controller. However, the elements made up of these production systems have a non-linear structure, resulting in a loss of performance and stability. Motivated by this key limitation of these research in [1]-[7], we have conceived the integration of non-linear control strategies, especially those called advanced control to improve the efficiency of the HRES. These strategies are mainly developed to follow the demanded power of each element composed of the global system, to use optimally the energy sources and to regulate the DC bus voltage of the HRES.

The voltage source inverter (VSI) is required in the production system for voltage and frequency regulation at the Point of Common Coupling (PCC). The performances obtained are closely evaluated in terms of the dynamic response time of the system, the steady-state error, and the total harmonic distortion (THD).

Furthermore, the nature of VSI yield voltage is intensely influenced by the disturbances of the load, for example sudden load change and nonlinear load. Subsequently, the performance of the control strategy is very dependent on the dynamic characteristics of the load. In the literature, several techniques have been proposed for the control of VSI in islanded micro-grid [2],[8]. In [6] - [8], a traditional PI controller has been explored to control the VSI operating in islanded micro-grid with a reasonably adjusted load condition. However, this control technique can not cover the substantial load variation (the yield voltage as a lot of the relentless state error could not ensure the robustness of the system and its THD is not acceptable due to the non-linear load). Reference [9] has presented a PI technique to control the VSI for a HRES composed of WT and PV panels. In this case, the frequency and voltage regulation were performed but the non-linear load and unbalanced load are not considered which will make the system unreliable. Recently, advanced controllers have been extensively applied to the VSI like the multi resonant control [10], integral resonant control [11], repetitive control [12], predictive controller [13] and feedback linearization [14]. However, these control strategies are reasonable for only adjusted load conditions, but not to cover the expansive load variation.

The sliding mode control (SMC) is a robust, nonlinear type controller that was initially introduced to control the variable structure systems [15]. Its main advantages are the guarantee of stability and robustness against external disturbances variations and parametric disturbances [16]. These properties make this technique suitable for the control of power converters system in an island micro-grid with non-linear loads [15]. In a variable structure system using SMC, it is found that PWM based SMC using equivalent control law is the most common and widely used approach for controlling the power converters in an islanded micro-grid [25],[26].

This study develops non-linear controllers with SMC for a hybrid system including boost dc-dc converter, bidirectional dc-dc buck-boost converter and VSI. The architecture of the proposed stand-alone HRES includes two renewable energy sources, the PMSG and PV array, and the energy storage devices (BESS) as presented in Fig.1. Each element in the block is interconnected through its power converter (dc-dc or ac/dc) controlled by its local control law and connected to the common dc bus. The PV array is connected through a boost dc-dc converter for tracking the maximum power point MPP by the MPPT technique. The wind subsystem involving a turbine equipped with a PMSG and a VSI to extract MPP from the VSWT. Furthermore, the battery has a bidirectional dc-dc converter, which adjusts the voltage levels and allows the charging and discharging of the storage device. On the other hand, the ac load has a VSI, which makes it possible, thanks to the control, to regulate the voltage and the frequency at the PCC in the presence of various conditions.

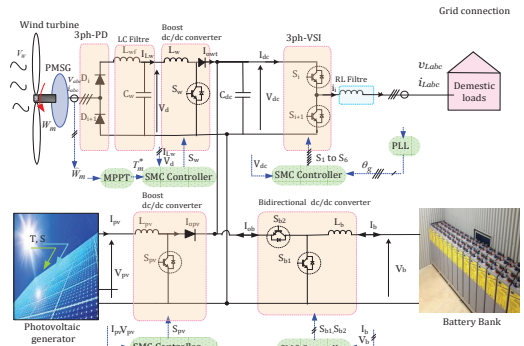


Fig. 1. Proposed configuration of HRES

II. Modeling components of the hybrid system

A. PV system model

A single diode model PV cell is used in this paper in order to describe with good accuracy of the electrical behavior of a PV cell. This model is widely used in many literatures [1],[2],[7], where the electric model consists of a generator current in parallel with a diode and a resistance shunt R_{sh} ; this set is itself in series with a second resistor R_s . The output current I_{pv} depending on the output voltage V_{pv} of a PV array is given by:

$$I_{pv} = N_p I_{ph} - N_s I_s \left\{ \exp \left[\frac{q}{nKT} \left(\frac{V_{pv}}{N_s} + \frac{R_s I_{pv}}{N_p} \right) - 1 \right] \right\} - \frac{N_p \left(\frac{V_{pv}}{N_s} + \frac{R_s I_{pv}}{N_p} \right)}{R_{sh}} \quad (1)$$

where I_{ph} is the photocurrent, I_s is the reverse saturation current, n is the ideality factor, q is the electron charge ($q = 1.6 \cdot 10^{-19}$), k the Boltzmann's constant ($k = 1.38 \cdot 10^{-23}$), and T is the temperature, R_s is the intrinsic series resistance, R_{sh} is the equivalent shunt resistance. N_s and N_p represent the number of modules in series and in parallel respectively. The PV array has 5 modules connected in series and 5 modules connected in parallel for providing 7.625 kW peak power in STC (Standard Test Conditions): Insolation (G) of 1 kW/m² and cell temperature (T) of 25°C. The output power-voltage-current characteristics, depending on the insolation and temperature, are presented in Fig. 2.

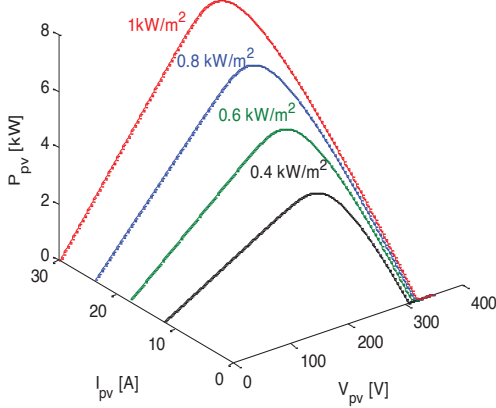


Fig. 2. P_{pv} - V_{pv} - I_{pv} output characteristics: (a) for different values of G at constant T of 25 °C

B. Wind turbine model

The mechanical power retrieved by the blades of a wind turbine is given by the following relationship [20]:

$$P_w = \frac{1}{2} \rho C_p(\lambda, \beta) A v_w^3 \quad (2)$$

where ρ is the air density (kg/m^3), v_w is the wind speed in m/s and C_p is the turbine rotor power coefficient. The speed ratio λ is dependent on rotor speed and wind speed, which can be given by:

$$\lambda = \frac{R w_m}{v_w} \quad (3)$$

where w_m and R is the rotor speed and radius of the wind turbine. From (2) and (3), we obtain the expression of mechanical torque generated by the wind turbine.

$$T_m = \frac{C_p(\lambda, \beta) \rho \pi R^5}{2 \lambda^3} w_m \quad (4)$$

The wind turbine is modeled by equation (4) in which only depends of variables wind turbine rotor speed w_m and the tip speed ratio λ . The wind turbine can produce maximum power when the coefficient of power is always at its maximum value, we have $C_p = C_{pmax}$ which corresponds to an optimum value of the tip speed ratio λ . In these conditions, the target optimum torque can be given by:

$$T_{m_opt} = k_{opt} (w_{m_opt})^2 \quad (5)$$

where

$$k_{opt} = \frac{1}{2} \rho A C_{p_{opt}} \left(\frac{R}{\lambda_{opt}} \right)^2 \quad (6)$$

Fig.3 shows the output characteristics generated by turbine blades depending on the rotation rotor speed at each wind speed, where the red curve represents the optimum target. It is noted from this figure that the optimality of power is achieved when the generator torque follows the optimum torque curve. The goal of the MPPT control is to allow the wind turbine to provide the maximum possible power given by this curve.

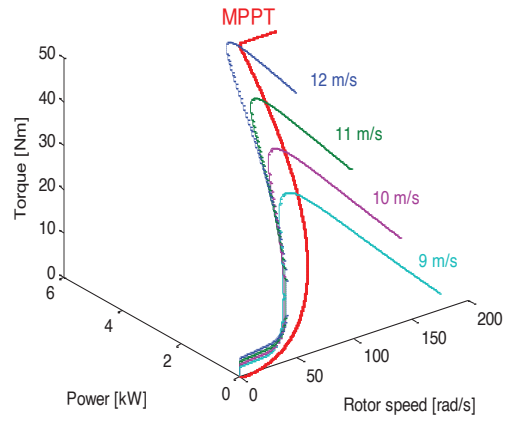


Fig. 3. Output characteristics generated by a turbine blade under different wind speeds

C. Battery model

The lead-acid battery is used as a storage device which is connected to a common dc link capacitor through a bidirectional buck-boost dc-dc converter. The equivalent model of this storage is composed of a perfect source voltage in series with a resistor as a constant resistance and the terminal voltage is described by [2].

III. Control strategies of the hybrid energy system

A. MPPT control

To optimize the production of electrical energy from the photovoltaic source regardless of the atmospheric conditions, the static converter is equipped with an MPPT control. Several methods of MPPT have been proposed in the literature, such as P&O method, Sliding Mode Controller (SMC) method, InCond method, fuzzy-neural method and General Regression Neural Network

[1]-[7],[18]. The most popular MPPT in this field are the P&O and InCond methods because they are simple and inexpensive.

In order to extract maximum power from the PV source, we must act on the boost converter by the action on the duty cycle. In our study, we chose the Adaptive P&O Algorithm based SMC.

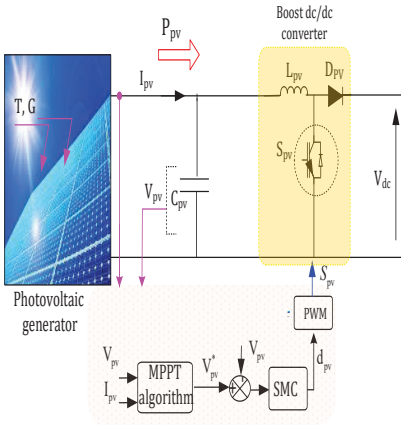


Fig. 4. Photovoltaic MPPT Control

The flow chart of this method is illustrated in Fig. 6. The principle of this method may be given as follows:

$$V(k) = V(k-1) + k_{pv} \cdot \text{sign}(\Delta P) \quad (7)$$

with

$$\Delta P_{pv} = P(k) - P(k-1) \quad (8)$$

where k_{pv} is adaptive step gain which depends of state variation of the power.

The computation of a state model is necessary for the synthesis of this control law. This requires the characterization of the system by a mathematical equation reflecting the behaviour of the PV-boost converter. The following equation is the mathematical representation of the relationship of the output of the PV and the input of the boost converter as shown in Fig.1 (if $R_s=0, R_{sh}=\infty$).

$$\dot{V}_{pv} = \frac{1}{C_{pv}} \left[I_{ph} - I_d \exp\left(\frac{V_{pv}}{V_t} - 1\right) \right] - \frac{I_{dc}}{C_{pv}} \cdot u \quad (9)$$

The steps to design an SMC controller for a dc-dc converter can be found in [19]-[21]. The following sliding surfaces as a linear combination of the state variables described as:

$$S = \alpha_1 x_1 + \alpha_2 x_2 + \alpha_3 x_3 \quad (10)$$

where $\alpha_1, \alpha_2,$ and α_3 represent the control parameters of the SMC, usually referred to as sliding coefficients, and $x_1, x_2,$ and x_3 denote the desired state feedback variables, which are defined as:

$$\begin{cases} x_1 = V_{pvref} - V_{pv} \\ x_2 = \frac{d(V_{pvref} - V_{pv})}{dt} \\ x_3 = \int (V_{pvref} - V_{pv}) dt \end{cases} \quad (11)$$

The control law of SMC for boost converter is of the form:

$$u = \begin{cases} 1 & \text{when } S_{pv} > 0 \\ 0 & \text{when } S_{pv} < 0 \end{cases} \quad (12)$$

In this paper, the SMC boost dc-dc converter operates at a constant switching frequency by employing PWM instead of Hysteresis-Modulation [21].

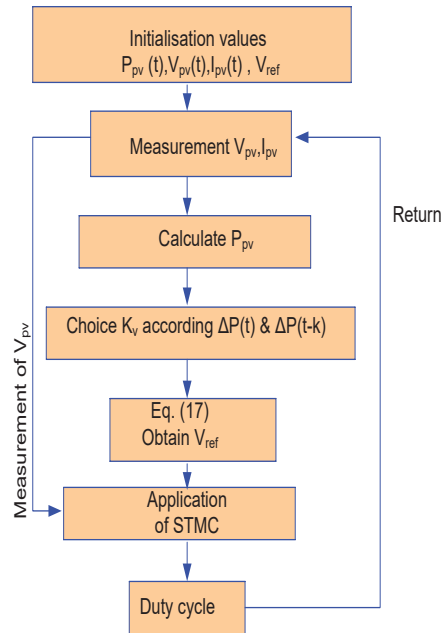


Fig. 5. Flow chart of the proposed APOAM

B. Control of PMSG

The wind turbine is controlled by a VSC with SVPWM, which imposes the voltages (v_{sa} , v_{sb} , v_{sc}) of the phases of PMSG.

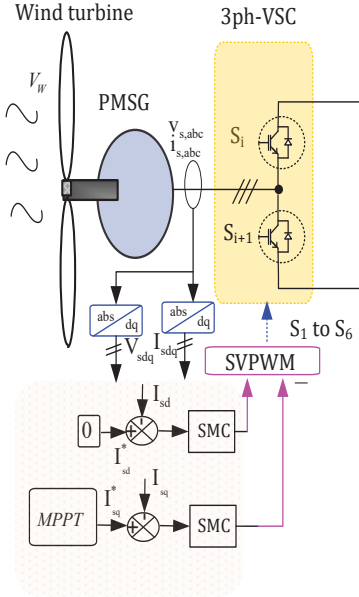


Fig. 6. Control of PMSG

We chose to control the torque given in equation (6). In this area, the SMC will be outlined, for the present control loops of Fig.1. Characterize the accompanying sliding surfaces

$$\begin{cases} S_{S1} = I_{sdref} - I_{sd} \\ S_{S2} = I_{sqref} - I_{sq} \end{cases} \quad (13)$$

where I_{sdref} , I_{sqref} are the reference variables for I_{sd} , I_{sq} , respectively. The control law is outlined forcing the sliding mode presence condition for surfaces $s_{S1}\dot{s}_{S1} < 0$.

The control input is chosen to have the structure as follows

$$\begin{cases} u_{S1} = u_{eqs1} + k_{S1} \cdot |S_{S1}|^\alpha \text{sgn}(S_{S1}) \\ u_{S2} = u_{eqs2} + k_{S2} \cdot |S_{S2}|^\alpha \text{sgn}(S_{S2}) \end{cases} \quad (14)$$

where k_{si} is a positive gain.

The equivalent control information is acquired from the invariance condition and given by the accompanying condition as $S_{si} = 0$ and $\dot{S}_{si} = 0 \Rightarrow u_{si} = u_{eqi}$. Condensing, the expression for the equivalent control u_{eqsi} terms can be resolved as:

$$\begin{cases} u_{eq1} = (R_s I_{sd} - \omega_e L_q I_{sq}) + L_d \dot{I}_{sdref} \\ u_{eq2} = \left(R_s I_{sq} + \omega_e \frac{L_d}{L_q} I_{sd} + \omega_e \Psi \right) + \dot{I}_{sqref} \end{cases} \quad (15)$$

C. BESS Control

The block diagram of the proposed control of the bidirectional buck-boost dc-dc converter using sliding mode current controller is shown in Fig. 7. The sliding surface is defined for the regulation of the input current of the buck-boost converter as follows.

$$S_b = \gamma_1 x_1 + \gamma_2 x_2 + \gamma_3 x_3 \quad (16)$$

where γ_1 , γ_2 , and γ_3 represent the control parameters of the SMC, usually referred to as sliding coefficients, and x_1 , x_2 , and x_3 denote the desired state feedback variables, which are defined as

$$\begin{cases} x_1 = I_{bref} - I_b \\ x_2 = \frac{d(I_{bref} - I_b)}{dt} \\ x_3 = \int (I_{bref} - I_b) dt \end{cases} \quad (17)$$

The parameters γ_1 , γ_2 , and γ_3 are positive values determined by the resolution of the differential equation using the root locations in order to have the convergence appropriate the sliding surface to zero. Similar to the control of the boost converter, the SMC buck-boost dc-dc converter operates at a constant switching frequency by employing PWM and its control law is given in equation (16).

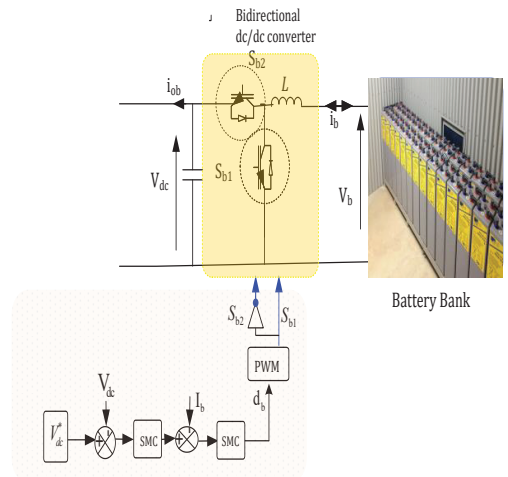


Fig. 7. Control of BESS

D. Stand-alone control mode VSC

Fig. 8 demonstrates the block diagram of the proposed stand-alone control mode. The sliding surface of this control is defined as follows.

$$\begin{cases} s_{m1} = V_{Ldref} - V_{Ld} \\ s_{m2} = V_{Lqref} - V_{Lq} \\ s_{m3} = I_{Ldref} - I_{Ld} \\ s_{m4} = I_{Lqref} - I_{Lq} \end{cases} \quad (18)$$

where V_{Ldref} , V_{Lqref} , I_{Ldref} , I_{Lqref} are the desired load current and voltage in d - and q -axes respectively. The goal of the proposed control calculation appears in Fig. 9 is to direct the consistent load voltage and recurrence within the sight of different conditions. To accomplish these destinations, the accompanying conditions are forced:

$$\begin{cases} V_{Ldref} = V_{LL} \\ V_{Lqref} = 0 \\ \theta = \omega t = 2\pi \cdot f \cdot t \end{cases} \quad (19)$$

where V_{LL} is the line-line load voltage and f is the load frequency, which is equal to 50 Hz. The control input is defined as follows:

$$\begin{cases} u_{m1} = u_{eqm1} + k_{m1} \cdot |s_{V_{Ld}}|^\alpha \cdot \text{sgn}(s_{m1}) \\ u_{m2} = u_{eqm2} + k_{m2} \cdot |s_{V_{Lq}}|^\alpha \cdot \text{sgn}(s_{m2}) \\ u_{m3} = u_{eqm3} + k_{m3} \cdot |s_{m3}|^\alpha \cdot \text{sgn}(s_{m3}) \\ u_{m4} = u_{eqm4} + k_{m4} \cdot |s_{m4}|^\alpha \cdot \text{sgn}(s_{m4}) \end{cases} \quad (20)$$

where k_{mi} is a positive gain.

The equivalent control input is obtained from the invariance condition and given by the accompanying condition as $S_{mi} = 0$ and $\dot{S}_{mi} = 0 \Rightarrow u_{mi} = u_{eqmi}$.

Therefore, the expression for the equivalent control terms u_{eqi} can be obtained as:

$$\begin{cases} u_{eqm1} = C_f \omega V_{Lq} + I_{Ld} \\ u_{eqm2} = -C_f \omega V_{Ld} + I_{Lq} \\ u_{eqm3} = V_{Ld} + L_f \cdot I_{Ld} - \omega \cdot L_f \cdot I_{Lq} \\ u_{eqm4} = V_{Lq} + L_f \cdot I_{Lq} + \omega \cdot L_f \cdot I_{Ld} \end{cases} \quad (21)$$

The objective of SMC is to guarantee the convergence of the operation points to predetermine sliding boundary. To verify the stability of the system, Lyapunov function candidates are used $s_{mi} \cdot \dot{s}_{mi} < 0$. At that point the range of k_{mi} can be determined as follows:

$$\begin{cases} k_{m1} > C_f |\Delta f_1|; k_{m2} > C_f |\Delta f_2| \\ k_{m3} > L_f |\Delta f_3|; k_{m4} > L_f |\Delta f_4| \end{cases} \quad (22)$$

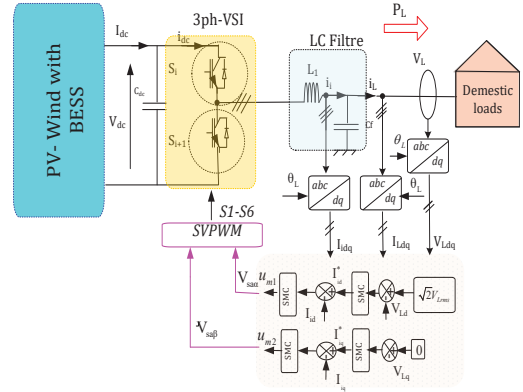


Fig. 8. Control VSC for stand-alone mode

IV. Simulation results

Different simulation results are used to analyze the dynamic performance of the HRES are presented in this work. The overall configuration shown in Fig. 1 of HRES is simulated by utilizing the *MATLAB/Simulink*. The dc-link voltage is controlled at 700 V. The distribution power of the HRES is based on the variable input source. Specifically, the wind speed increases from 10m/s to 14m/s at $t=0.3s$. The solar irradiation increased from 0.6 kW/m² to 1 kW/m² at $t=0.2s$ and decreased from 1kW/m² to 0.8 kW/m² at $t=0.4s$, while the temperature is constant at 25°C.

The simulation is executed to illustrate the excellent performance of the proposed HRES controller under following different cases: case 1) Linear load is connected to the system at $t = 0s$ and is disconnected at $t = 0.3s$; case 2) nonlinear load (three-phase diode rectifier, $L_{load} = 10 \text{ mH}$, $R_{load} = 50 \Omega$) is connected to system at period $t \in [0.2 \ 0.3]s$; case 3) Increased of resistive load by 100% at period $t \in [0.3 \ 0.4]$; case 4) unbalanced resistive load ($R_{Lb} = 87.5 \% R_{La}$, $R_{Lc} = 75 \% R_{La}$) at period $t \in [0.4 \ 0.5]$. Fig. 9 shows the control performance of PV system with solar irradiance variations whose data sets. It is seen from this figure that the PV system controller tracks the MPPs of the solar energy regardless of the rapidly changing wind speed

and load condition. The comparison between the APOAM and P&O algorithm of power response is illustrated in Fig. 10. It is clear from this figure that the proposed algorithm is effective in changing weather conditions because the work point of the system oscillates weakly around the maximum power point.

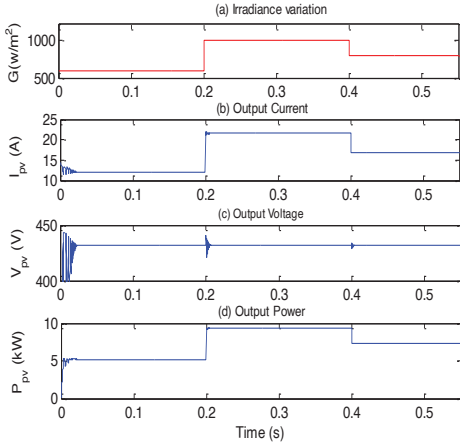


Fig. 9. Control performance PV system in SAM operation

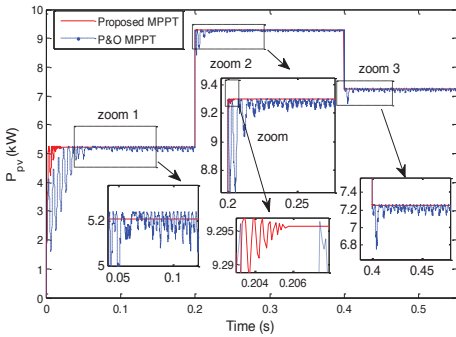


Fig. 10. Comparison between the APOAM and P&O algorithm of power response

Fig. 11 shows the response of the wind turbine system in SAM operation. The wind speed V_w , the power coefficient, the measured and reference rotor speed of $PMSG$, the reference and output of torque of the wind turbine, the wind turbine output power are shown in Fig.12. The simulation results demonstrate that the proposed controller operates the wind generator in the maximum power point regardless of variation in the environmental conditions and load types tested.

Fig. 12 shows the response of the $BESS$ system. This figure shows battery voltage (V_b), state of charge of battery ($SOC\%$), battery current (I_b) and output of power of the battery. It is observed, at period $t \in [0, 0.2]$ the aggregate of wind and PV produced power is not adequate to supply the heap request to supply the load

demand. Under this circumstance, the battery discharges with a positive current. At period $t \in [0, 0.2]$ the power request by the load is not as much as the power created by the sources. In this way, the battery is charged of a negative current. The reference dc current and measured dc current are as shown in Fig. 12 (b). It is observed that the measured battery current follows the reference current to supply load demand by charging or discharging this storage.

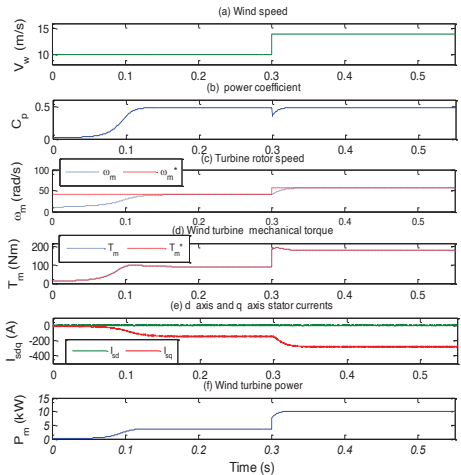


Fig. 11. Control performance wind turbine system

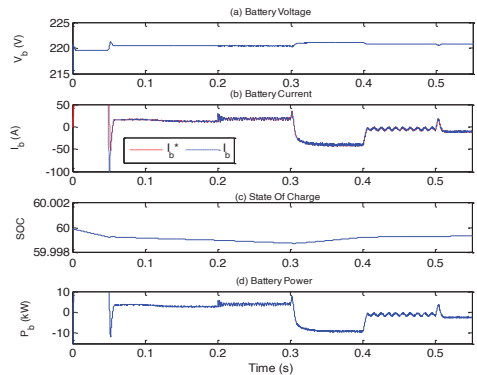


Fig. 12. Control performance of the BESS

Fig.13 shows the simulation results of the proposed control technique under in this test, respectively of load voltages ($v_{L,abc}, V_{Ldq}$), load currents ($i_{L,abc}, I_{Ldq}$), output currents of VSC ($i_{i,abc}, I_{idq}$), the dc bus voltage and active power of load. The VSC able to regulate the voltage level of local ac load at 230 V and the frequency at 50 Hz as shown in Fig.15. Obviously, it can be observed from the simulation results that the proposed SMC based

control strategy affirms the fast dynamic response and voltage tracking performance with small steady-state error and lower part under different load types (balanced load, unbalanced load, and nonlinear load).

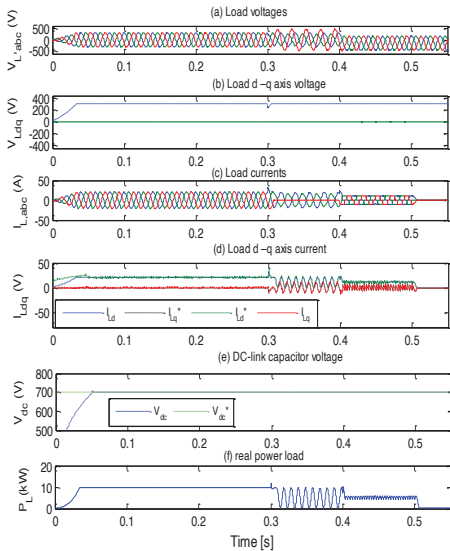


Fig. 13. Control performance of VSC

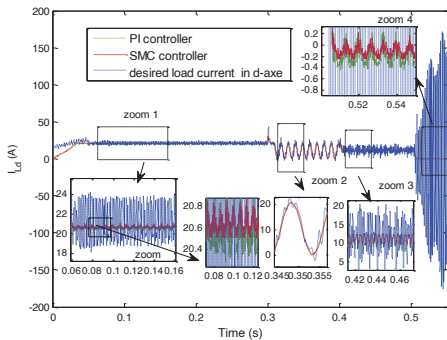


Fig. 14. Performance of direct current control

To better appreciate the upsides of the proposed approach, we propose a progression of comparable tests with the traditional PI control as shown in Fig. 14. It can be seen from this figure and Table I that the proposed control system has more points of interest in wording in terms of voltage regulation, fast steady-state error, and low harmonic distortion.

TABLE I
SUMMARY OF RESULTS

Cases	Parameters	PI controller	SMC controller
1	THDi(0-0.2s), (VLabc)	3.73%, (220, 220.4, 220.1)	0.04%, (220, 220, 220)
2	THDi(0.2-0.3s),	10.6%,	10.51%,

	(VLabc)	(220,8 220,8, 220,8)	(220 219,9 219,9)
3	THDi(0.3-0.4s), (VLabc)	4.74%, (220,2 220,3, 220,3)	1.2%, (220 220 220.1)
4	THDi(0.4-0.5s) (VLabc)	3.91%, (233,4,224,7, 203,8)	3.1%, (233.1 224,2 203.1)

V. Conclusion

The main objective of this work is to contribute to the design of an effective and robust control strategy for a HRES in isolated sites. A new approach based on the non-linear STC is proposed in order to improve the energy efficiency of HRES. The performance of the proposed method for controlling various converters associated to the HRES such as variations in wind speed, temperature and solar irradiation, irregularity of the load, power demand, unbalanced load, and nonlinear load, was verified and compared with the conventional PI controllers. The main contribution and advantages of the proposed system under all conditions are as follows:

- The proposed MPPT algorithm APOAM STSMC control can enhance the performance and durability of the PV system and the setting time response of the boost converter comparing with P&O algorithm.
- The proposed SMC has the advantages of fast dynamic response, less overshoot, faster disturbances rejection time, small steady-state error with good accuracy and very low THD value compared with the conventional PI controller in all cases.

It is concluded from the simulation results that, the proposed approach improves the quality and provides a stable operation of HRES. The robustness and the stability of the whole system are widely improved using SMC than other classical approaches.

References

- [1] Bouthaina Madaci, Rachid Chenni, Erol Kurt, Kamel Eddine Hemsas. Design and control of a stand-alone hybrid power system. International Journal of Hydrogen Energy.2016; 41(29): 12485-12496.
- [2] S.G. Malla, C.N Bhende. Voltage control of stand-alone wind and solar energy system. International Journal of Electrical Power & energy systems. 2014; 56:361-373.
- [3] Caisheng Wang, Hashem Nehrir. Power Management of a Stand-Alone Wind/Photovoltaic/Fuel Cell Energy System. IEEE Transactions on Energy Conversion. 2008; 23(3)-957-967.
- [4] S. Tamalouzi, N. Benyahia, T. Rekioua , D. Rekioua , R. Abdessemed. Performances analysis of WT-DFIG with PV and fuel cell hybrid power sources system associated with hydrogen storage hybrid energy system, International Journal of Hydrogen Energy. 2016; 41(45): 21006-21021.
- [5] Amin Mirzaei, Majid Forooghi, Ali Asghar Ghadimi, Amir Hossein, Abolmasoumi, Mohammad Reza Riah. Design and construction of a charge controller for stand-alone PV/battery hybrid system by using a new control strategy and power management. Solar Energy, 2017; 149:132-144.

- [6] C. N. Bhende, Mishra, Siva Ganesh Malla. Permanent Magnet Synchronous Generator-Based Standalone Wind Energy Supply System. *IEEE Transactions on Sustainable Energy*. 2011; 2(4):
- [7] BENADLI, Ridha et all. Control and simulation of a standalone photovoltaic-wind with a fuel cell and battery storage. *Journal of Electrical Engineering*, 2020, vol. 20, no 5, p. 6-6.
- [8] Ghada Boukettaya, Lotfi Krichen. A dynamic power management strategy of a grid connected hybrid generation system using wind, photovoltaic and Flywheel Energy Storage System in residential applications. *Energy*.2014. 71:148-159.
- [9] Despoina I. Makrygiorgou, Antonio T. Alexandridis. Distributed stabilizing modular control for stand-alone microgrids. *Applied Energy*, *In press, corrected proof*, 2017.
- [10] A.Hasanzadeh, C.S. Edrington, B. Maghsoudlou, F. Fleming, H. Mokhtari. Multi-loop linear resonant voltage source inverter controller design for distorted loads using the linear quadratic regulator method. *IET Power Electronics*, 2012, 5(6): 841–851.
- [11] Alessandro Lidozzi, Giovanni Lo Calzo, Luca Solero, Fabio Crescimbin. Integral-resonant control for stand-alone voltage source inverters. *IET Power Electronics*. 2014.7(2) :271-278.
- [12] Alessandro Lidozzi; Chao Ji, Luca Solero, Fabio Crescimbin; Pericle Zanchetta. Load-Adaptive Zero-Phase-Shift Direct Repetitive Control for Stand-Alone Four-Leg VSI. *IEEE Transactions on Industry Applications*. 2016; 52(6): 4899-4908.
- [13] W. Razia Sultanaa, Sarat Kumar Sahooa, Sukruedee Sukchaib, S. Yamunaa, D. Venkatesha. A review on state of art development of model predictive control for Renewable Energy applications. *Renewable and Sustainable Energy Reviews*. 2017; 76: 391-406.
- [14] Dong-Eok Kim, Dong-Choon Lee. Feedback Linearization Control of Three-Phase UPS Inverter Systems. *IEEE Transactions on Industrial Electronics*. 2010; 57(3):963-968.
- [15] S. Spurgeon, C. Edwards, *Sliding Mode Control: Theory and Practice*. Taylor and Francis London: 1998.
- [16] VI. Utkin. Sliding mode control design principles and applications to electric drives. *IEEE Transactions on Industrial Electronics*.1993; 40(1):23-36.
- [17] Miloud Rezkallah, Member, Abdelhamid Hamadi, Ambrish Chandra, Fellow, Bhim Singh. Real-Time HIL Implementation of Sliding Mode Control for Standalone System Based on PV Array Without Using Dumpload. *IEEE Transactions On Sustainable Energy*, 2015; 6(4): 1389-1398.
- [18] BENADLI, Ridha, KHIARI, Brahim, et SELLAMI, Anis. Predictive current control strategy for a three-phase grid connected photovoltaic-wind hybrid system. In : *2016 7th International Renewable Energy Congress (IREC)*. IEEE, 2016. p. 1-6.
- [19] Utkin V, Guldner J, Shi J. *Sliding mode control in electromechanical systems*. 2nd ed. London: 882 Taylor and Francis; 2009.
- [20] Ali H. Kasem Alaboudy, Ahmed A. Daoud, Sobhy, S. Desouky, Ahmed A. Salem. Converter 899 controls and flicker study of PMSG-based grid connected wind turbines. *Ain Shams Engineering Journal*. 2013; 4(1): 75-91.
- [21] Ya-Xiong Wang, Fei-Fei Qin, Kai Ou, Young-Bae Kim, "Sliding-Mode-Control-Based DC/DC Converters Design and Implementation for Hybrid Proton Exchange Membrane Fuel Cell/Battery Power System", 9th International Conference on Power Electronics-ECCE Asia, June 2015.

